Linear Enhancement of Spin–Orbit Torque and Absence of Bulk Rashba Spin Splitting in Perpendicularly Magnetized $[Pt/Co/W]_n$ Superlattices

Zhihao Yan[1,2], Zhengxiao Li[1,2], Lujun Zhu[3], Xin Lin[1,2], and Lijun Zhu[1,2*]

[1]*State Key Laboratory of Semiconductor Physics and Chip Technologies, Institute of Semiconductors, Chinese Academy of Sciences, Beijing 100083, China*

[2]*Center of Materials Science and Optoelectronics Engineering, University of Chinese Academy of Sciences, Beijing 100049, China*

[3]*College of Physics and Information Technology, Shaanxi Normal University, Xi'an 710062, China*

(Received 3 April 2025; accepted manuscript online 7 July 2025)

The development of magnetic heterostructures with strong perpendicular magnetic anisotropy (PMA), strong spin–orbit torques (SOTs), low impedance, and good integration compatibility at the same time is central for high-performance spintronic memory and computing applications. Here, we report the development of the PMA superlattice $[Pt/Co/W]_n$ that can be sputtered-deposited on commercial oxidized silicon substrates and has giant SOTs, strong uniaxial PMA of $\approx 9.2\,\mathrm{Merg/cm^3}$, and rigid macrospin performance. The damping-like and field-like SOTs of the $[Pt/Co/W]_n$ superlattices exhibit a linear increase with the repeat number n and reach the giant values of 225% and −33% (two orders of magnitude greater than that in clean-limit Pt) at $n = 12$, respectively. The damping-like SOT is also of the opposite sign and much greater in magnitude than the field-like SOT, regardless of the number n. These results clarify that the spin current that generates SOTs in the $[Pt/Co/W]_n$ superlattices arises predominantly from the spin Hall effect rather than bulk Rashba spin splitting, providing a unified understanding of the SOTs in these superlattices. We also demonstrate deterministic switching in thicker-than-50-nm PMA $[Pt/Co/W]_{12}$ superlattices at a low current density. This work establishes the $[Pt/Co/W]_n$ superlattice as a compelling material candidate for ultra-fast, low-power, long-retention nonvolatile spintronic memory and computing technologies.

DOI: 10.1088/0256-307X/42/9/090701 CSTR: 32039.14.0256-307X.42.9.090701

1. Introduction. It has been a core topic of spintronics to develop magnetic heterostructures that have high spin–orbit torques (SOTs), low impedance, strong perpendicular magnetic anisotropy (PMA), and good integration compatibility at the same time, for ultra-fast, low-power, long-retention nonvolatile spintronic memory and computing technologies.[1–7] However, the SOT efficiency of the conventional spin Hall metal/ferromagnet bilayers is usually low; e.g., the damping-like (DL) SOT efficiency (ξ^j_{DL}) is only 0.02 for Pt/ferromagnet bilayers with clean-limit Pt (resistivity $\approx 7\,\mu\Omega\cdot\mathrm{cm}$[8]) and 0.05–0.1 for those with dirtier Pt.[9–15] Recently, a symmetry-broken spin–orbit superlattice,[15,16] which stacks identical trilayers of the spin-current generator/magnet/symmetry-breaking layer with a repeat number n, is proposed to increase the damping-like and field-like (FL) SOT efficiencies, ξ^j_{DL} and ξ^j_{FL}, by n times when the spin Hall effect (SHE) is the only source of the spin current that generates SOTs in these superlattices.

However, the linear enhancement of the SOTs has never been achieved in any PMA superlattices that are technologically desirable for enhanced data retention time and integration density, leaving the technological benefits and the SOT mechanisms of the superlattice as critical open questions. Demonstration of the effects would require good identity of the repeats across the large thickness of the superlattices and rigid macrospin behavior for reliable SOT quantification,[1,11] which is challenging for most material systems due to possible degradation of layer smoothness and PMA induced, e.g., by strain relaxation during stacking of superlattices. For instance, the $[Pt/Co/MgO]_n$ superlattice degrades substantially at large repeat numbers in terms of smoothness, resistivity, and saturation magnetization,[15] leading to much slower SOT enhancement than expected linear-in-n scaling. Ham *et al.*[17] fabricated $[Pt/Co/W]_n$ superlattices that disobeyed the macrospin model and suggested a non-monotonic variation of SOTs with n, low upper-limit SOT efficiencies ($\xi^j_{\mathrm{DL}} \approx 0.4$ and $\xi^j_{\mathrm{FL}} \approx 0.7$), and a dominant SOT source from stacking-collectively-induced "bulk Rashba spin splitting".

In this work, we, for the first time, developed the $[Pt/Co/W]_n$ superlattices with strong PMA and rigid macrospin behaviors at low magnetic fields. With this ability, we demonstrate that both damping-like and field-like SOTs of the $[Pt/Co/W]_n$ superlattices exhibit a reasonable linear-in-n enhancement towards infinity, with the damping-like torque being always of the opposite sign and much greater in magnitude than the field-like torque. These results clarify that the SOTs in the $[Pt/Co/W]_n$ su-

*Corresponding author. Email: ljzhu@semi.ac.cn

© 2025 Chinese Physical Society and IOP Publishing Ltd. All rights, including for text and data mining, AI training, and similar technologies, are reserved.

perlattice arise from SHE rather than stacking-collectively-induced bulk Rashba-type spin splitting.

2. Sample Details. For this study, we fabricated $5 \times 60\,\mu m^2$ Hall bars of $[Pt(2.5)/Co(0.8)/W(1.5)]_n$ superlattices (numbers in the brackets are layer thicknesses in nanometers; the repeat number n = 1, 4, 6, 8, 10, and 12, respectively) sputter-deposited on thermally oxidized silicon substrates and protected by $MgO(1.6)/TaO_x$ bilayers [Figs. 1(a) and 1(b)]. A thickness of 0.8 nm is chosen for the Co layers as a compromise between interfacial PMA and spin dephasing.[18–20] The Pt layers are made to be 2.5 nm thick to generate strong SOTs without making the whole superlattice ($n \leq 12$) too thick to etch (overetching damages the photoresist). Each superlattice was preceded by a 1 nm Ta seed layer to enhance adhesion with the substrate. For electrical measurements, the samples were patterned into $5 \times 60\,\mu m^2$ Hall bars by photolithography and argon ion milling, followed by the deposition of Ti (5 nm)/Pt(150 nm) contacts. No intentional annealing was performed.

Cross-sectional high-angle annular dark-field scanning transmission electron microscopy characterizations suggest that the $[Pt/Co/W]_n$ superlattices have very good layer smoothness for $n \leq 6$, but slightly increased roughness for larger n [Fig. 1(a)]. The first harmonic Hall voltage (HHV) hysteresis loops as a function of the perpendicular magnetic field (H_z) suggest good PMA [Fig. 1(c)]. In Fig. 1(d), we plot the Pt resistivity ρ_{xx}, saturation magnetization M_s, PMA field H_k, and uniaxial PMA energy $K_u = M_s H_k/2$ of the Co layers as a function of n in the superlattices. The value of ρ_{xx} varies from 54 μΩ·cm to 39 μΩ·cm as estimated from the conductance enhancement of the $Ta(1)/[Pt/Co/W]_n/MgO(1.6)/Ta(1.5)$ stack, relative to n times the conductance of a control stack lacking a Pt layer, i.e., $Ta(1)/Co(0.8)/W(1.5)/MgO(1.6)/Ta(1.5)$. These superlattices exhibit high M_s values of 1340 ± 36 emu/cm^3, strong H_k values of 13.8 ± 1.1 kOe, and giant uniaxial PMA energy values of 9.2 ± 0.5 Merg/cm^3 (much greater than that of bulk PMA ferrimagnets FeTb[21] and optimized Ta/CoFeB/MgO[22]).

3. Linear-in-n Enhancement of SOTs. The SOT efficiencies in the $[Pt/Co/W]_n$ superlattices are carefully characterized using HHV measurements in the low-field macrospin regime by taking into account thermoelectric effects.[15,23] The in-phase first and out-of-phase second HHVs, $V_{1\omega}$ and $V_{2\omega}$, are collected as a function of the swept longitudinal (H_x) and transverse (H_y) magnetic fields while applying a sinusoidal electric field E of 30 kV/m onto the Hall bar oriented along the x axis [Fig. 1(b)]. For all the superlattices in this study, $V_{1\omega}$ exhibits a 100% remanent ratio during the sweeping of H_z [Fig. 1(c)] and perfect parabolic scaling during the sweeping of H_x and H_y, while $V_{2\omega}$ exhibits excellent linear scaling with the in-plane fields [Figs. 2(a) and 2(b)]. These characteristics consistently reveal the rigid macrospin behavior[1] of these superlattices in the studied regime of in-plane magnetic fields (e.g., $H_x, H_y < 1.5$ kOe for the superlattice with $n = 12$). To further ensure macrospin behavior and avoid any occurrence of multidomain states during HHV measurements, we always saturate the superlattices into $+M_z$ ($-M_z$) states using a sufficiently large positive (negative) H_z before collecting $V_{1\omega}$ and $V_{2\omega}$ as functions of in-plane magnetic fields swept only in low ranges. Note that fulfilling rigid macrospin behaviors in studied magnetic field regimes is critical for reliable analysis of SOTs because otherwise, the HHV technique would not apply at all. The superlattice with $n = 12$ does show some steplike switching during H_z scanning in Fig. 1(c) likely due to a sizable distribution of nucleation and/or pinning field; however, this should not affect macrospin analysis in the regime far away from magnetization switching.

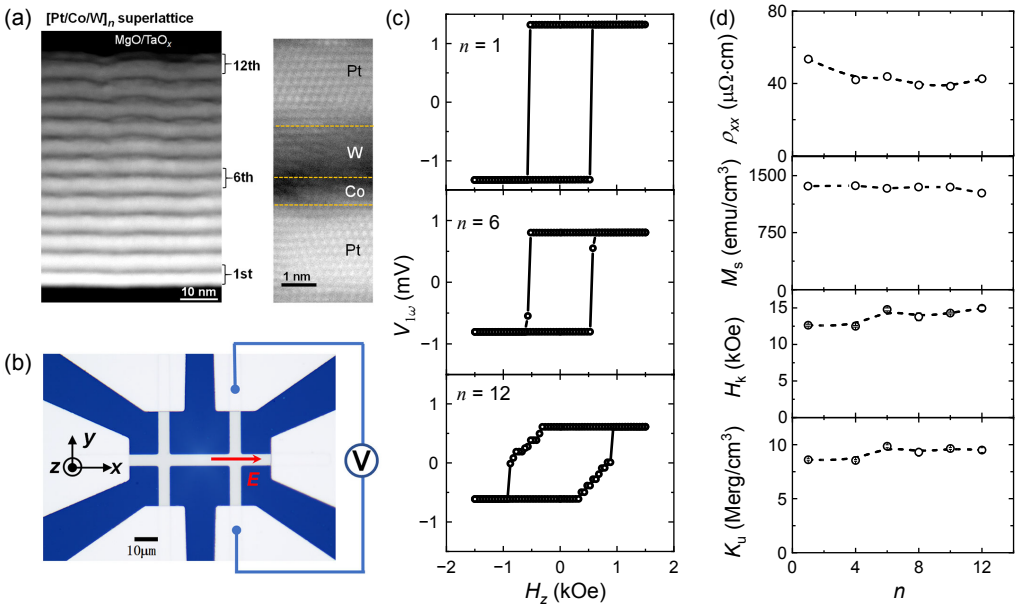

Fig. 1. (a) High-angle annular dark-field scanning transmission electron microscopy images of the $[Pt/Co/W]_{12}$ superlattice. (b) Optical microscopy image of the Hall bar device. (c) First HHV vs. perpendicular magnetic field. (d) Resistivity, saturation magnetization, PMA field, and uniaxial PMA energy of the $[Pt/Co/W]_n$ superlattice with varying repeat number n.

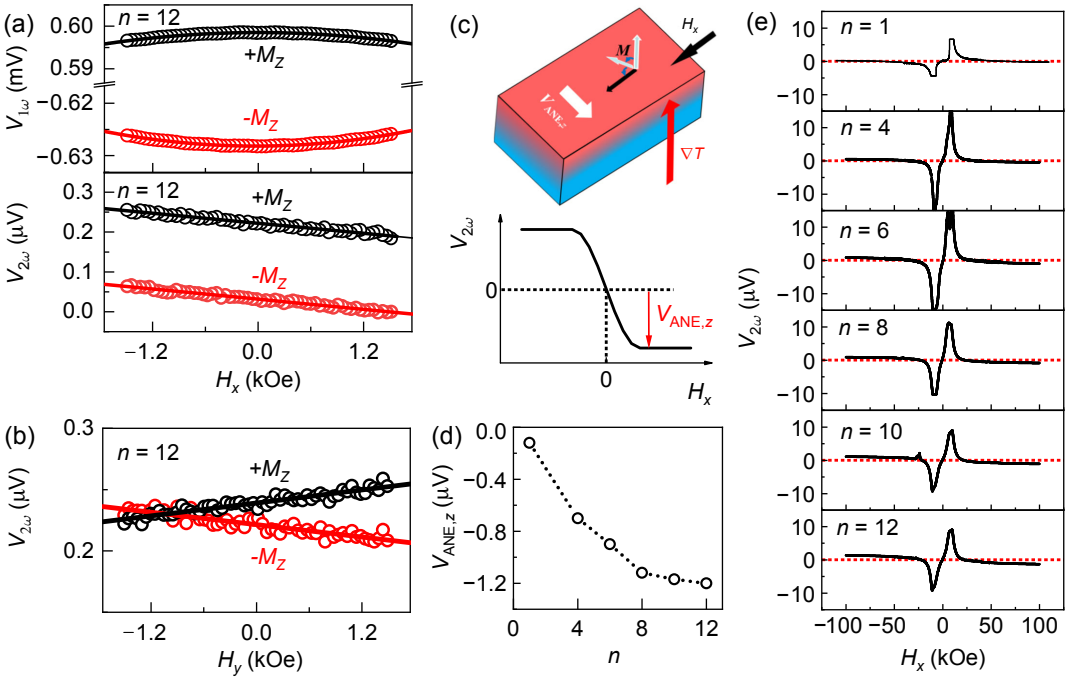

Fig. 2. First and second HHVs ($V_{1\omega}$, $V_{2\omega}$) of the $[Pt(2.5)/Co(0.8)/W(1.5)]_{12}$ superlattices plotted as a function of (a) the longitudinal magnetic field H_x and (b) the transverse magnetic field H_y. (c) Schematic of the generation and measurement of the anomalous Nernst voltage of PMA samples. (d) Anomalous Nernst voltage and (e) $V_{2\omega}$ vs. H_x for the $[Pt/Co/W]_n$ superlattices with different n.

Based on the rigid macrospin behavior of the samples, we determine H_k, the damping-like SOT field H_{DL}, and the field-like SOT field H_{FL} from the parabolic scaling of $V_{1\omega}$ and linear scaling of $V_{2\omega}$ with in-plane magnetic fields, i.e.,

$$V_{1\omega} \approx V_{AHE}\left[1 - \frac{H_{x(y)}^2}{2H_k^2}\right], \tag{1}$$

$$H_{DL} = -2\frac{\frac{\partial V_{2\omega}}{\partial H_x}}{\frac{\partial^2 V_{1\omega}}{\partial^2 H_x}} - 2H_k\frac{V_{ANE,z}}{V_{AHE}}, \tag{2}$$

$$H_{FL} = -2\frac{\frac{\partial V_{2\omega}}{\partial H_y}}{\frac{\partial^2 V_{1\omega}}{\partial^2 H_y}} - H_{Oe}, \tag{3}$$

where V_{AHE} is the anomalous Hall voltage that is extracted from the dependence of $V_{1\omega}$ on H_z in Fig. 1(c). H_{Oe} is the transverse Oersted field exerted on the Co layers by the in-plane charge current in other layers and can be estimated as $(j_{Pt}d_{Pt} - j_W d_W)/2$, with $j_{Pt(W)}$ and $d_{Pt(W)}$ being the current density and layer thickness of the Pt(W) layers (see detailed discussions in our previous work [16]). From fitting the scaling of $V_{1\omega}$ with H_x and H_y to Eq. (1), H_k is determined to be 13.8 ± 1.0 kOe for the $[Pt/Co/W]_n$ superlattices with different n. $V_{ANE,z}$ is the anomalous Nernst voltage due to the perpendicular thermal gradient and equal to the value of $V_{2\omega}$ when magnetization is fully aligned along the current direction by H_x of 90 kOe [see Fig. 2(c) for a schematic depiction and supporting information from Ref. [21] for deriving correlation of $V_{ANE,z}$ and $V_{2\omega}$]. Here, the perpendicular thermal gradient within superlattices arises from different thermal dissipation at bottom and outer surfaces (SiO_2 vs air). [21–23] As shown in Figs. 2(d) and 2(e), $V_{ANE,z}$ becomes increasingly significant as n increases. We note that low-field $V_{2\omega}$ data from wide-range field scans [Fig. 2(e)] typically contain complicated multi-domain features against macrospin behavior and should not be used for any macrospin analyses of SOTs (e.g., HHV analysis).

With the values of H_{DL} and H_{FL} determined using Eqs. (2) and (3), the damping-like and field-like SOT efficiencies per electric field, ξ^E_{DL} and ξ^E_{FL}, are calculated as [9]

$$\xi^E_{DL(FL)} = \left(\frac{2e}{\hbar}\right)\frac{\mu_0 M_s t H_{DL(FL)}}{E}, \tag{4}$$

where e is the elementary charge, $\hbar$ the reduced Planck's constant, μ_0 the permeability of vacuum, and t is the total thickness of the magnetic layer ($t = 0.8n$ nm for the $[Pt/Co/W]_n$ superlattice). As shown in Fig. 3(a), both ξ^E_{DL} and ξ^E_{FL} linearly increase in magnitude as n increases, while ξ^E_{FL} is of the opposite sign and 3.5 times smaller in magnitude than ξ^E_{DL}.

Since we have only measured negligible SOTs in the control samples Ta(1)/Co(0.8)/W(1.5)/MgO(1.6)/Ta(1.5) and Ta(1)/Co(0.8)/MgO(1.6)/Ta(1.5), the SOTs of the $[Pt/Co/W]_n$ superlattices should be predominantly from the SHE of the Pt layers. This suggests that the W layers in the $[Pt/Co/W]_n$ superlattices are unable to generate detectable spin flow due to their low spin Hall conductivity, insufficient layer thickness, and/or poor crystallinity [Fig. 1(a)] despite a thick metastable β-phased W layer being reported to have a negative spin Hall ratio. [24] This allows us to accurately calculate the damping-like and field-like SOT efficiencies per current density, ξ^j_{DL} and ξ^j_{FL}, of the $[Pt/Co/W]_n$ superlattices using

$$\xi^j_{DL(FL)} = \rho_{xx}\xi^E_{DL(FL)}. \tag{5}$$

As summarized in Fig. 3(b), both $\xi^j_{\rm DL}$ and $\xi^j_{\rm FL}$ linearly increase in magnitude with growing n, i.e., $\xi^j_{\rm DL} = 0.173n$ and $\xi^j_{\rm FL} = -0.027n$. The enhancement rate $\frac{\xi^j_{\rm DL}}{n} = 0.173$ for the $[\rm Pt(2.5)/Co(0.8)/W(1.5)]_n$ (ρ_{xx} = 39–54 μΩ·cm) is slightly greater than that of in-plane magnetized Pt(2)/Co(0.8)/MgO ($\xi^j_{\rm DL} = 0.15$, $\rho_{xx} = 60\,\mu\Omega\cdot$cm),[16] mainly due to the greater Pt thickness.

The linear-in-n enhancement of the SOTs and the field-like SOT being of the opposite sign and much smaller in magnitude than the damping-like SOT agree well with the SHE being the dominant origin of the SOTs in the symmetry-broken spin–orbit superlattices[15,16] and reveal negligible stacking-collectively induced contributions of SOTs or spin currents in the $[\rm Pt(2.5)/Co(0.8)/W(1.5)]_n$ superlattices. This is consistent with the linear increase of the damping-like and field-like SOTs with n in the in-plane anisotropy $[\rm Pt_{0.75}Cu_{0.25}/Co/Ta]_n$ superlattices, the absence of SOTs in symmetry-preserved $[\rm Pt/Co]_n$ superlattices,[16] and the theoretical prediction of no bulk Rashba-type spin splitting for $[\rm Pt/Co/W]_n$ with a W thickness of ≥0.74 nm.[17] While a previous HHV experiment on $[\rm Pt(1)/Co(0.6)/W(\leq 1)]_n$ superlattices[17] claimed a strong bulk Rashba spin splitting from non-monotonic scaling of SOTs with n and a field-like torque that is of the same sign but almost twice in magnitude compared to that of damping-like torque, those samples disobeyed the macrospin model, which is the base of HHV analysis, as revealed by remarkable hysteresis in $V_{2\omega}$ signals as a function of swept in-plane magnetic fields. The HHV analyses of those $[\rm Pt(1)/Co(0.6)/W(\leq 1)]_n$ samples also employed a large planar Hall correction[25,26] that has been suggested to cause errors by researchers including developers of this "correction" and should be avoided.[13,15,27–31]

4. Practical Impacts. Finally, such $[\rm Pt/Co/W]_n$ superlattices are technologically compelling. As compared in Fig. 3(c), the $[\rm Pt/Co/W]_n$ has remarkably higher SOT efficiency than other metallic systems, including Pt-X alloys, Ta, and W, while keeping a relatively low resistivity. In Fig. 3(d), we demonstrate that the $[\rm Pt/Co/W]_n$ superlattices make it possible to switch rather thick 3d ferromagnets with strong PMA (≈9.6 Merg/cm^3) using a relatively low current density (about 2.0×10^7 A/cm^2 under $H_x = 3$ kOe). This is in contrast to the conventional heavy metal/ferromagnet bilayer scheme, for which a Co layer is unlikely to be switchable by interfacial SOT before the blowout of the device due to Joule heating when the thickness is several nm (e.g., 9.6 nm), and can hardly maintain PMA when the effective thickness is above 1.5 nm. The ability of the superlattice to effectively switch a large-volume magnetic layer is interesting for spintronic applications where the magnetic layer has to be thick enough to maintain PMA and/or thermal stability when the lateral

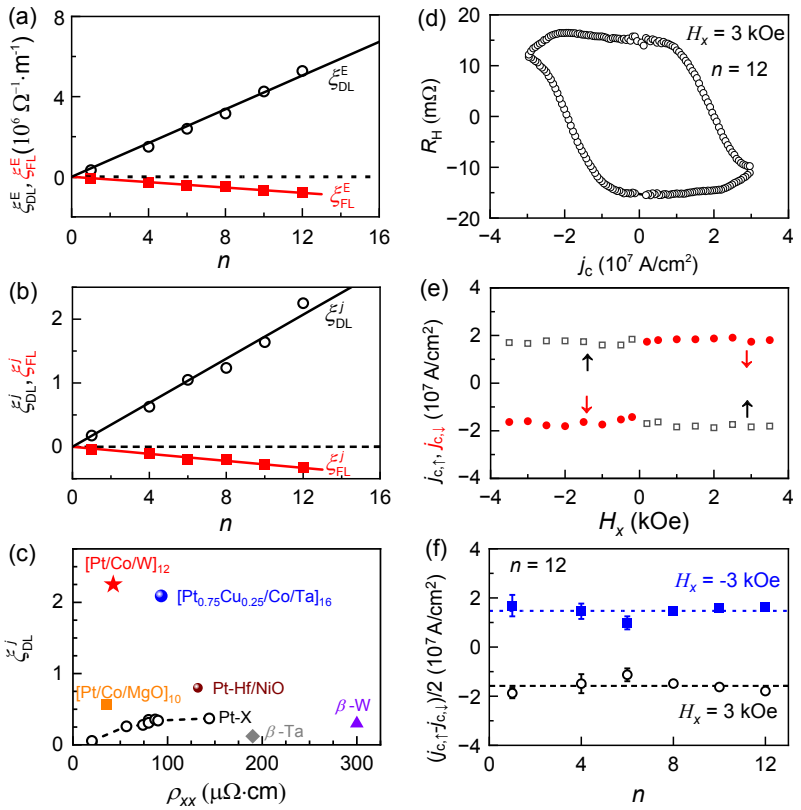

Fig. 3. Damping-like and field-like SOT efficiencies (a) per electric field and (b) per current density for the $[\rm Pt(2.5)/Co(0.8)/W(1.5)]_n$ superlattices, indicating a linear increase of the SOTs with the repeat number n. (c) Comparison of resistivity of strong SOT materials. (d) Hall resistance vs. charge current density of the $[\rm Pt(2.5)/Co(0.8)/W(1.5)]_{12}$ under an in-plane magnetic field of $H_x = 3$ kOe, showing deterministic switching at an average current density of about 2.0×10^7 A/cm^2. (e) Dependence on H_x of the upward and downward switching current densities ($j_{c,\uparrow}$ and $j_{c,\downarrow}$) for the $[\rm Pt(2.5)/Co(0.8)/W(1.5)]_{12}$ superlattices. (f) Average switching current density $(j_{c,\uparrow} - j_{c,\downarrow})/2$ under $H_x = 3$ kOe (black) and $H_x = -3$ kOe (blue) for the $[\rm Pt(2.5)/Co(0.8)/W(1.5)]_n$ superlattices with different repeat numbers n.

size scales down to tens of nanometers. Since power scales with $(1/\xi^j_{\rm DL})^2$, such $[{\rm Pt/Co/W}]_n$ superlattices should have n^2 times lower power consumption to generate a given spin torque strength than the corresponding conventional magnetic bilayer with the same total magnetic volume. As shown in Fig. 3(e), the switching current density of the $[{\rm Pt/Co/W}]_n$ superlattices only exhibits a weak dependence on the in-plane magnetic field, which is similar to previous reports of Co-based PMA samples (see Fig. S1 in Ref. [32] for data on Pt-X/Co bilayers). For the $[{\rm Pt/Co/W}]_n$ superlattices with different n, the average switching current density remains essentially unchanged [Fig. 3(f)] due to identical superlattice repeats despite an increase in thickness of the magnetic layers. It should be clarified that large thicknesses of these magnetic layers would certainly increase total write current and energy compared to single-repeat Pt/Co/W trilayers.

Therefore, such $[{\rm Pt/Co/W}]_n$ superlattice can be utilized to develop self-torqued magnetic tunnel junctions and superlattice racetracks for memory,[3,4] computing,[5,6,33] and microwave emitter[5] applications that require low power, long endurance, low impedance, and large magnetic volume for enhanced thermal stability[15,16,34,35] or signal output. The coupling of different Co layers via dipolar and Ruderman–Kittel-Kasuya–Yosida (RKKY) interactions across the very thin heavy metal layers (e.g., W 1.5 nm/Pt 2 nm) and the identical spin current-generating layer within each repeat is expected to assure coherent SOT switching of the entire superlattice with identical repeats. Note that RKKY interaction of magnetic layers separated by nonmagnetic spacers of several nanometers in thickness (typically 2–4.5 nm) has been reported to enable significant interlayer Dzyaloshinskii–Moriya interaction,[36–39] while the dipole field can enable magnetic field-free SOT switching of the magnetic free layers of magnetic tunnel junctions across a distance of up to tens of nanometers.[40]

5. Conclusion. In summary, we have, for the first time, developed $[{\rm Pt/Co/W}]_n$ superlattices with strong PMA and rigid macrospin behavior at the same time. With this ability, we demonstrate a linear enhancement of both damping-like and field-like SOTs of the PMA $[{\rm Pt/Co/W}]_n$ superlattices with the repeat number n, with $\xi^j_{\rm DL} = 225\%$ and $\xi^j_{\rm FL} = -33\%$ at $n = 12$. The highest n value of practical superlattices is limited by accumulating structural roughness. We also find that the damping-like torque is always much greater than the field-like torque, regardless of the number of n. These results clarify that the SOTs in the $[{\rm Pt/Co/W}]_n$ superlattice arise from the SHE, which establishes a unified understanding of the mechanism of SOTs in these superlattices. Deterministic switching is, for the first time, achieved in thicker-than-50 nm PMA $[{\rm Pt/Co/W}]_{12}$ superlattices with a low current density of about 2.0×10^7 A/cm^2. These results establish the $[{\rm Pt/Co/W}]_n$ superlattice with strong PMA, giant SOTs, low impedance, and good integration compatibility as a compelling material candidate for ultra-fast, low-power, long-retention nonvolatile spintronic memory and computing technologies.

Data Availability. The original data is available from the correspondence author upon reasonable request.

Acknowledgements. This work was supported by the National Key Research and Development Program of China (Grant No. 2022YFA1204000), the Beijing National Natural Science Foundation (Grant No. Z230006), and the National Natural Science Foundation of China (Grant Nos. 12304155 and 12274405).

References

[1] Zhu L J 2023 *Adv. Mater.* **35** 2300853
[2] Miron I M, Garello K, Gaudin G, Zermatten P J, Costache M V, Auffret S, Bandiera S, Rodmacq B, Schuhl A, and Gambardella P 2011 *Nature* **476** 189
[3] Liu L Q, Pai C F, Li Y, Tseng H W, Ralph D, and Buhrman R A 2012 *Science* **336** 555
[4] Zhu L J, Zhu L J, Shi S J, Ralph D C, and Buhrman R A 2020 *Adv. Electron. Mater.* **6** 1901131
[5] Grollier J, Querlioz D, Camsari K, Everschor-Sitte K, Fukami S, and Stiles M 2020 *Nat. Electron.* **3** 360
[6] Luo Z C, Hrabec A, Dao T P, Sala G, Finizio S, Feng J X, Mayr S, Raabe J, Gambardella P, and Heyderman L J 2020 *Nature* **579** 214
[7] Cubukcu M, Boulle O, Mikuszeit N, Hamelin C, Brächer T, Lamard N, Cyrille M C, Buda-Prejbeanu L, Garello K, and Miron I M 2018 *IEEE Trans. Magn.* **54** 1
[8] Sagasta E, Omori Y, Isasa M, Gradhand M, Hueso L E, Niimi Y, Otani Y, and Casanova F 2016 *Phys. Rev. B* **94** 060412
[9] Nguyen M H, Ralph D C, and Buhrman R A 2016 *Phys. Rev. Lett.* **116** 126601
[10] Liu L Q, Moriyama T, Ralph D C, and Buhrman R A 2011 *Phys. Rev. Lett.* **106** 036601
[11] Zhu L J, Ralph D C, and Buhrman R A 2021 *Appl. Phys. Rev.* **8** 031308
[12] Zhu L J, and Buhrman R A 2019 *Phys. Rev. Appl.* **12** 051002
[13] Zhu L J, Sobotkiewich K, Ma X, Li X Q, Ralph D C, and Buhrman R A 2019 *Adv. Funct. Mater.* **29** 1805822
[14] Zhu L J, Zhu L J, Shi S J, Sui M L, Ralph D C, and Buhrman R A 2019 *Phys. Rev. Appl.* **11** 061004
[15] Zhu L J, Li J W, Zhu L J, and Xie X Y 2022 *Phys. Rev. Appl.* **18** 064052
[16] Lin X, Zhu L J, Liu Q B, and Zhu L J 2023 *Nano Lett.* **23** 9420
[17] Ham W S, Ho T H, Shiota Y, Iino T, Ando F, Ikebuchi T, Kotani Y, Nakamura T, Kan D, Shimakawa Y, Moriyama T, Im E, Lee N J, Kim K W, Hong S C, Rhim S H, Ono T, and Kim S 2023 *Adv. Sci.* **10** 2206800
[18] Ghosh A, Auffret S, Ebels U, and Bailey W 2012 *Phys. Rev. Lett.* **109** 127202
[19] Taniguchi T, Yakata S, Imamura H, and Ando Y 2008 *IEEE Trans. Magn.* **44** 2636
[20] Zhu L J and Ralph D C 2023 *Nat. Commun.* **14** 1778
[21] Liu Q B, Zhu L J, Zhang X S, Muller D A, and Ralph D C 2022 *Appl. Phys. Rev.* **9** 021402
[22] Ikeda S, Miura K, Yamamoto H, Mizunuma K, Gan H D, Endo M, Kanai S, Hayakawa J, Matsukura F, and Ohno H 2010 *Nat. Mater.* **9** 721
[23] Avci C O, Garello K, Gabureac M, Ghosh A, Fuhrer A, Alvarado S F, and Gambardella P 2014 *Phys. Rev. B* **90** 224427
[24] Pai C F, Liu L Q, Li Y, Tseng H W, Ralph D C, and Buhrman R A 2012 *Appl. Phys. Lett.* **101** 122404
[25] Hayashi M, Kim J, Yamanouchi M, and Ohno H 2014 *Phys. Rev. B* **89** 144425

[26] Torrejon J, Kim J, Sinha J, Mitani S, Hayashi M, Yamanouchi M, and Ohno H 2014 *Nat. Commun.* **5** 4655
[27] Karimeddiny S, Cham T M J, Smedley O, Ralph D C, and Luo Y K 2023 *Sci. Adv.* **9** eadi9039
[28] Zhu L J and Buhrman R A 2021 *Phys. Rev. Appl.* **15** L031001
[29] Lau Y C and Hayashi M 2017 *Jpn. J. Appl. Phys.* **56** 0802B5
[30] Zhu L J, Ralph D C, and Buhrman R A 2019 *Phys. Rev. Lett.* **122** 077201
[31] Zhu L J, Ralph D C, and Buhrman R A 2018 *Phys. Rev. Appl.* **10** 031001
[32] Zhu L J, Ralph D C, and Buhrman R A 2021 *Phys. Rev. Appl.* **15** 024059
[33] Liu Q B, Liu L, Xing G Z, and Zhu L 2024 *Nat. Commun.* **15** 2978
[34] Watanabe K, Jinnai B, Fukami S, Sato H, and Ohno H 2018 *Nat. Commun.* **9** 663
[35] Jinnai B, Watanabe K, Fukami S, and Ohno H 2020 *Appl. Phys. Lett.* **116** 160501
[36] Han D S, Lee K L, Hanke J P, Mokrousov Y, Kim K W, Yoo W, Hees Y L W, Kim T W, Lavrijsen R, You C Y, Swagten H J M, Jung M H, and Kläui M 2019 *Nat. Mater.* **18** 703
[37] Avci C O, Lambert C, Sala G, and Gambardella P 2021 *Phys. Rev. Lett.* **127** 167202
[38] Kim T, Cha I H, Kim Y J, Kim J W, Stashkevich A, Roustingé Y, Belmeguenai M, Chérif S M, Samardak A S, and Kim Y K 2021 *Nat. Commun.* **12** 3280
[39] Liang S X, Chen R Y, Cui Q R, Zhou Y J, Pan F, Yang H X, and Song C 2023 *Nano Lett.* **23** 8690
[40] Garello K, Yasin F, Hody H, Couet S, Souriau L, Sharifi S H, Swerts J, Carpenter R, Rao S, Kim W, Wu J, Sethu K K V, Pak M, Jossart N, Crotti D, Furnémont A, and Kar G S 2019 *Symposium on VLSI Circuits,* Kyoto, Japan, p. T194